

COMPLEXLY ZONED FIBROUS TOURMALINE, CRUZEIRO MINE, MINAS GERAIS, BRAZIL: A RECORD OF EVOLVING MAGMATIC AND HYDROTHERMAL FLUIDS

BARBARA L. DUTROW[§] AND DARRELL J. HENRY

Department of Geology and Geophysics, Louisiana State University, Baton Rouge, Louisiana 70803, U.S.A.

ABSTRACT

Silver-gray tourmaline fibers intergrown with a deep pink elbaite host from the Cruzeiro mine, Minas Gerais, Brazil, provide evidence for the compositional evolution of magmatic and hydrothermal fluids involved in pegmatite formation. Optical and back-scattered electron imaging, together with detailed microanalysis, establish that the fibers, 0.05–0.3 mm in width, are complexly zoned and developed in four distinct generations marked by discrete compositions and replacement textures. Fiber growth is punctuated by periods of dissolution. The first generation, preserved in the fiber interior, is a dark blue foitite; the blue-gray second generation varies from Fe-rich elbaite to Li-rich schorl, and the third generation is a yellowish-green “fluor-elbaite”. Volumetrically the most abundant, generation-three fibers poikiloblastically replace the earlier generations as well as the host. A fourth generation of fibrous tourmaline fills fractures that cut all previous generations and the host, but is unrelated to growth of the previous fibers. Compositionally, last generation is indistinguishable from the second-generation Li-rich schorl fibers. Textural and compositional discontinuities of each generation record periods of stability followed by reaction(s) in which the tourmaline was initially unstable, partially dissolved owing to interaction with fluids, and then redeveloped in response to interactions with evolving orthomagmatic or hydrothermal fluids. The general progression of the first three generations implies that reacting fluids were generally undergoing fractionation, becoming successively enriched in Na, Li, Ca, and F during late crystallization of the pegmatite. The composition was reset to a Li-rich schorl during late-phase fracturing. Crystal-chemical constraints such as F – X-site vacancy avoidance control part of the compositional variability observed. In this multistage tourmaline sample, individual fibers exhibit the most chemically complex compositions yet recorded, and reflect the dramatic complexity of fluid evolution involved in their crystallization.

Keywords: fibrous tourmaline, tourmaline dissolution, foitite, elbaite, fluids, Cruzeiro mine, Minas Gerais, Brazil.

SOMMAIRE

Des générations de tourmaline fibreuse en intercroissance avec une elbaïte rose foncé, provenant de la mine Cruzeiro, province de Minas Gerais, au Brésil, permettent de reconstruire l'évolution de la phase fluide orthomagmatique ou hydrothermale accompagnant la cristallisation de la pegmatite. Les images optiques et les images résultant de la rétrodiffusion d'électrons, avec les résultats de microanalyses, montrent que les fibres, d'une largeur de 0.05 à 0.3 mm, sont zonées de façon complexe. Elles se sont développées en quatre générations distinctes marquées par des sauts de composition et des textures de remplacement. La croissance des fibres est ponctuée par des intervalles de dissolution. La première génération, préservée à l'intérieur des fibres, est une foitite bleu foncé. La deuxième génération, gris-bleu, varie d'elbaïte ferrique à schorl lithinifère, et la troisième génération est une “fluor-elbaïte” vert jaunâtre. Cette dernière est la plus volumineuse; elle englobe de façon poecilitique les fibres précoces et la tourmaline hôte. Une quatrième génération de fibre remplit les fissures qui recoupent les trois générations antérieures, mais elle semble sans relation avec celles-ci. Du point de vue composition, la dernière génération rejoint la seconde (schorl lithinifère). Les discontinuités texturales et compositionnelles marquant chaque génération témoignent de périodes de stabilité suivies de réactions au cours desquelles la tourmaline, instable au départ, est en partie dissoute suite à une interaction avec la phase fluide, et ensuite redéveloppée en réponse aux interactions avec la phase fluide en évolution, soit d'origine orthomagmatique ou bien hydrothermale. La progression ordonnée en composition des trois premières générations fait penser que les fluides responsables étaient en voie de fractionnement, devenant par ce fait progressivement enrichis en Na, Li, Ca, et F au cours des stades tardifs de cristallisation de la pegmatite. La composition a ensuite été modifiée pour cristalliser un schorl lithinifère le long des fissures tardives. Des contraintes cristallographiques, par exemple l'incompatibilité de F et de lacunes sur le site X, exercent un contrôle partiel de la variabilité des compositions observées. Au cours de cette croissance épisodique, les fibres individuelles enregistrent les compositions les plus complexes qui soient connues, et illustrent ainsi la complexité dramatique du schéma d'évolution de la phase fluide accompagnant leur cristallisation.

(Traduit par la Rédaction)

Mots-clés: tourmaline fibreuse, dissolution, foitite, elbaïte, fluides, mine Cruzeiro, Minas Gerais, Brésil.

INTRODUCTION

The tourmaline group is characterized by extensive chemical substitutions, and thus compositionally diverse members. This chemical complexity makes tourmaline a valuable indicator of changes in its local chemical environment. In addition, it is a relatively stable mineral that preserves much of the textural and chemical signatures of earlier periods of growth. Consequently, tourmaline is exceedingly useful for tracking the compositional evolution of igneous and metamorphic rocks, and can often serve as a monitor of fluid infiltration. Numerous studies have demonstrated the utility of tourmaline in these environments as a petrogenetic indicator mineral (*e.g.*, Henry & Guidotti 1985, Henry & Dutrow 1992, Dutrow *et al.* 1999, London 1999, and many others).

Although tourmaline commonly exhibits a prismatic morphology, it is also one of the nearly 400 minerals that form fibers *sensu stricto* (Skinner *et al.* 1988). Fibrous tourmaline has long been recognized, but there are relatively few studies that define its composition, and even fewer that investigate its petrogenetic potential. Many examples of fibrous tourmaline develop in granitic pegmatites, a geological environment noted for evolving fluids. These occurrences provide an opportunity to investigate the composition of tourmaline fibers in a changing environment of growth and to evaluate their utility in monitoring this environment.

A detailed micro-analytical investigation was undertaken on a sample from the Cruzeiro mine, Governador Valadares, Minas Gerais, Brazil, in order to chemically characterize the fibrous tourmaline, to define the complexity of zoning present in single fibers, to provide information on growth history of the fibers, and to evaluate the role of tourmaline as a monitor of fluid evolution in pegmatitic environments.

BACKGROUND INFORMATION

The general formula for tourmaline can be expressed as $XY_3Z_6(T_6O_{18})(BO_3)_3V_3W$ (Hawthorne & Henry 1999). The relatively large *X* site contains Na, Ca, K, and vacancies ($^{\square}$); the two distinct octahedral sites, *Y* and *Z*, are occupied by a variety of divalent, trivalent and tetravalent cations, and Si with lesser Al dominates the tetrahedrally coordinated *T* site. The triangular *B* site is occupied exclusively by B, whereas the two anionic sites, *V* and *W*, contain OH^- , F^- and O^{2-} . Of particular importance to the proper classification of tourmaline is the fact that F exclusively enters the *W* site, and O^{2-} tends to partition into this site. In turn, the presence of dominant O^{2-} in the *W* site mandates local order in the distribution of cations at the *Y* and *Z* sites (Hawthorne 1996). The chemical diversity and structural requirements of tourmaline produce a large number of possible end-member species that have recently been reclassified in accordance with current knowledge of element

partitioning among tourmaline sites (Hawthorne & Henry 1999). Fibrous tourmaline falls into several of these categories. Table 1 summarizes the end-member species that are most important for this investigation.

Earlier investigators of fibrous tourmaline referred to them by various descriptive names such as "bugs nest", "whiskers", "filiform", "mountain leather" or "tourmaline asbestos" (*e.g.*, Coelho 1948, Bantly 1964, Mitchell 1964, Furbish 1968, Novák & Žák 1970, Dietrich 1985). Fibrous tourmaline has been shown to nucleate on a wide variety of substrates in many of geological settings. For example, fibrous tourmaline has been found associated with coarse-grained elbaite and schorl in miarolitic cavities in granitic pegmatites (*e.g.*, Bantly 1964, Pezzotta *et al.* 1996, Novák 1998), with quartz veins cutting schists, gneisses, or pegmatites (*e.g.*, Rama Swamy & Iyengar 1937, Mitchell 1964, Novák & Žák 1970, Šrein *et al.* 1997), within tourmalinized vugs in low-grade pyrophyllite deposits (Furbish 1968), as patches in altered and mineralized volcanic rocks (*e.g.*, Foit *et al.* 1989) or, most commonly, as fracture fillings in previously broken tourmaline crystals, where the fibers act as a sealing agent (*e.g.*, Mitchell 1964, Lyckberg & Hawthorne 1997). Typically, the fibers are distinctly different in color than the host tourmaline; in some cases, they exhibit a color change over the length of the fiber that reflects compositional variation (*e.g.*, Pezzotta *et al.* 1996).

In one of the earliest studies, Iyengar (1937) used wet-chemical techniques to show that the fibrous to semi-fibrous tourmaline from an undefined locality in Mysore State corresponds to alkali-deficient, aluminous schorl. Novák & Žák (1970) found that white asbestiform tourmaline from a quartz vein cutting graphite

TABLE 1. IMPORTANT TOURMALINE SPECIES ASSOCIATED WITH FIBROUS TOURMALINE

Species	(X)	(Y ₃)	(Z ₆)	T ₆ O ₁₈	(BO ₃) ₃	V ₃	W
Alkali tourmaline							
Elbaite	Na	Li _{1.5} Al _{1.5}	Al ₆	Si ₆ O ₁₈	(BO ₃) ₃	(OH) ₃	(OH)
"Fluor-Elbaite"*	Na	Li _{1.5} Al _{1.5}	Al ₆	Si ₆ O ₁₈	(BO ₃) ₃	(OH) ₃	(F)
"Oxy-Elbaite"*	Na	LiAl ₂	Al ₆	Si ₆ O ₁₈	(BO ₃) ₃	(OH) ₃	(O)
Schorl	Na	Fe ²⁺ ₃	Al ₆	Si ₆ O ₁₈	(BO ₃) ₃	(OH) ₃	(OH)
Dravite	Na	Mg ₃	Al ₆	Si ₆ O ₁₈	(BO ₃) ₃	(OH) ₃	(OH)
Olenite	Na	Al ₃	Al ₆	Si ₆ O ₁₈	(BO ₃) ₃	(O) ₃	(OH)
Calcic tourmaline							
Liddicoatite	Ca	Li ₂ Al	Al ₆	Si ₆ O ₁₈	(BO ₃) ₃	(O) ₃	(F)
Uvite	Ca	Mg ₃	Al ₆	Si ₆ O ₁₈	(BO ₃) ₃	(O) ₃	(F)
X-site-vacant tourmaline							
Rossmannite	\square	LiAl ₂	Al ₆	Si ₆ O ₁₈	(BO ₃) ₃	(O) ₃	(OH)
Foitite	\square	Fe ²⁺ Al	Al ₆	Si ₆ O ₁₈	(BO ₃) ₃	(O) ₃	(OH)
Magnesiofoitite	\square	Mg ₂ Al	Al ₆	Si ₆ O ₁₈	(BO ₃) ₃	(O) ₃	(OH)

* Species in quotation marks are not currently recognized as valid end-members by IMA, but are suggested as being appropriate by Hawthorne & Henry (1999).

schist is dravite with $Mg/(Mg + Fe) = 0.95$. Hyalophane, magnesian chlorite and pyrite, reflecting a local Mg-rich environment, accompany this asbestiform dravite.

More recently, investigators have begun to characterize the compositional variability developed in fibrous tourmaline. Foit *et al.* (1989) described fibrous zoned tourmaline associated with dumortierite in altered volcanic rocks as alkali-deficient schorl to foitite. Šrein *et al.* (1997) found that hair-like tourmaline occurring in late hydrothermal quartz veins is oscillatorily zoned Fe-rich dravite with significant amounts of Ca and Ti. Modreski *et al.* (1997) established that acicular to fibrous tourmaline from the Brumado magnesite deposit in Brazil has a range of compositions from dravite to uvite to magnesiofoitite. Novák (1998) characterized fibrous blue dravite that forms a subsolidus reactant at the margins between Li-poor pegmatites and Ca-, Mg-rich rocks such as marbles and serpentinites in the Moldanubicum, Czech Republic. Pezzotta *et al.* (1996) noted that in a pegmatite pocket from Elba, tourmaline fibers nucleated exclusively at the analogous pole of the elbaite–schorl substrate, where they crystallized into miarolitic cavities of the pegmatite dike, a growth pattern that suggests a genetic relationship between the fibers and late-stage fluids. These fibers are unzoned, alkali-deficient and Fe–Al-rich, and classified as foitite ($\square_{0.63}Na_{0.36}Ca_{0.01}$) $(Li_{0.33}Fe^{2+}_{1.52}Mg_{0.19}Ti_{0.01}Al_{0.86})Al_6Si_6O_{18}(BO_3)_3(OH)_4$. Aurisicchio *et al.* (1997) described similar fibers of X-site-deficient schorl and foitite nucleating on the analogous poles of coarse elbaite–olenite crystals from other bodies of pegmatite on Elba, and attributed fiber development to growth during late-stage fluid evolution, and to fluid infiltration associated with subsequent fracturing. Lyckberg & Hawthorne (1997) found dark orange-brown fibers of tourmaline associated with quartz, albite, muscovite, beryl and garnet in a gem pegmatite from the Alabashka Pegmatite Field, Ural Mountains, Russia. These fibers also have a foitite composition, and are related to the latest stage of pegmatite pocket formation.

GEOLOGY OF THE TOURMALINE-BEARING PEGMATITE

The fibrous tourmaline sample used in this study is from the Cruzeiro granitic pegmatites of Minas Gerais, Brazil (R. Van Wagoner, pers. commun.). This world-famous locality has produced gem-quality elbaite crystals and sheet muscovite (Cassedanne *et al.* 1980). The deposit consists of three subvertical dikes of granitic pegmatite that have sharply defined contacts with the host quartzite of the Serra da Safira sequence (Federico *et al.* 1998). The dikes, ranging from 8 to 60 meters wide, exhibit symmetrical mineralogical, textural and chemical zoning around a quartz core. The mineralogical and textural zonation consists of a border zone, wall zone, intermediate zone, pockets and a core zone. Mineralogically, the pegmatite is comprised predominantly of quartz, feldspar, muscovite and tourmaline, with mi-

nor beryl, almandine garnet and niobotantalates at the border zone and spodumene, lepidolite, amblygonite, spessartine garnet and beryl at the intermediate zones and pockets (Cassedanne *et al.* 1980, Federico *et al.* 1998). With the exception of minor garnet, no other ferromagnesian minerals appear to develop coevally with tourmaline. Many of the minerals in the pegmatite exhibit warping or fracturing (Cassedanne *et al.* 1980). Tourmaline is typically black at the border zone of the pegmatite and becomes color-zoned to green, green-blue and pink in the intermediate zones and pockets. Cassedanne *et al.* (1980) described massive deep rose to red elbaite locally with “asbestos-like” tourmaline in the pockets (see their Fig. 5), similar to those of our sample. The general compositional trends of the tourmaline in the pegmatite bodies are along the dravite–schorl join at the border, wall and external to medium intermediate zones, and along the schorl–elbaite joins at the internal intermediate zones and pockets. Relative to the outer zones of the pegmatite, tourmaline of the internal intermediate zones and pockets exhibits a significant increase in Li, YAl , F, Mn and Zn, and a decrease in Fe and Mg. Color-zoned tourmaline of the pockets typically features chemical zoning such that proportions of YAl and $^X\square$ increase, and Mn and F decrease toward the rim. Federico *et al.* (1998) considered the compositional trends of the tourmaline to reflect the chemical evolution of the pegmatite melt–fluid system.

CHARACTERIZATION OF THE SAMPLE

The sample of fibrous tourmaline consists of abundant silver-gray tourmaline fibers aligned parallel to the *c* axis of the host pink tourmaline crystal (Fig. 1). The fibers are typically 0.05–0.30 mm in width and 5.0–20.0 mm in length. Locally, the host and fibers are cut by fractures that contain a later generation of dark gray fibrous tourmaline. Nucleation points for the fibers are along the margin of the pink tourmaline, or at fractures where reactive fluids gained access to the crystal.

Analytical techniques

Thin sections were made both parallel and perpendicular to the *c* axis of the fibers in order to establish the textural and chemical relationships between the fibers and the pink tourmaline host. Optical and back-scattered electron (BSE) imaging establishes the complex nature of these fibers (Figs. 2–4). These images, in turn, were used as a base map for the position of detailed microanalyses.

Electron-microprobe analyses were done on the fibers and the host tourmaline by wavelength-dispersion spectrometry (WDS) using an automated JEOL 733 electron microprobe at Louisiana State University. Analytical conditions were: accelerating potential 15 kV, and beam current 5–10 nA, 1–2 μm focussed electron beam. Well-characterized synthetic and natural silicates

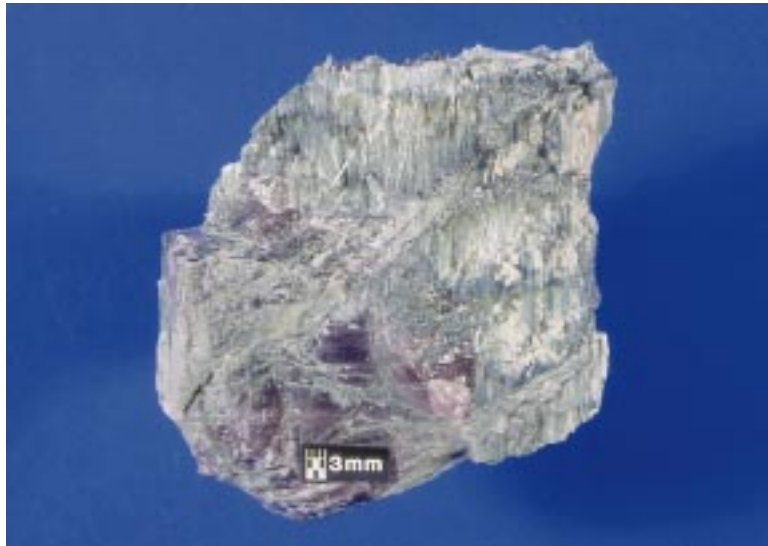


FIG. 1. Silver-gray fibrous tourmaline replacing and cutting the pink elbaite host. Darker gray fibrous tourmaline veins cut all earlier generations of fibrous tourmaline and the host.

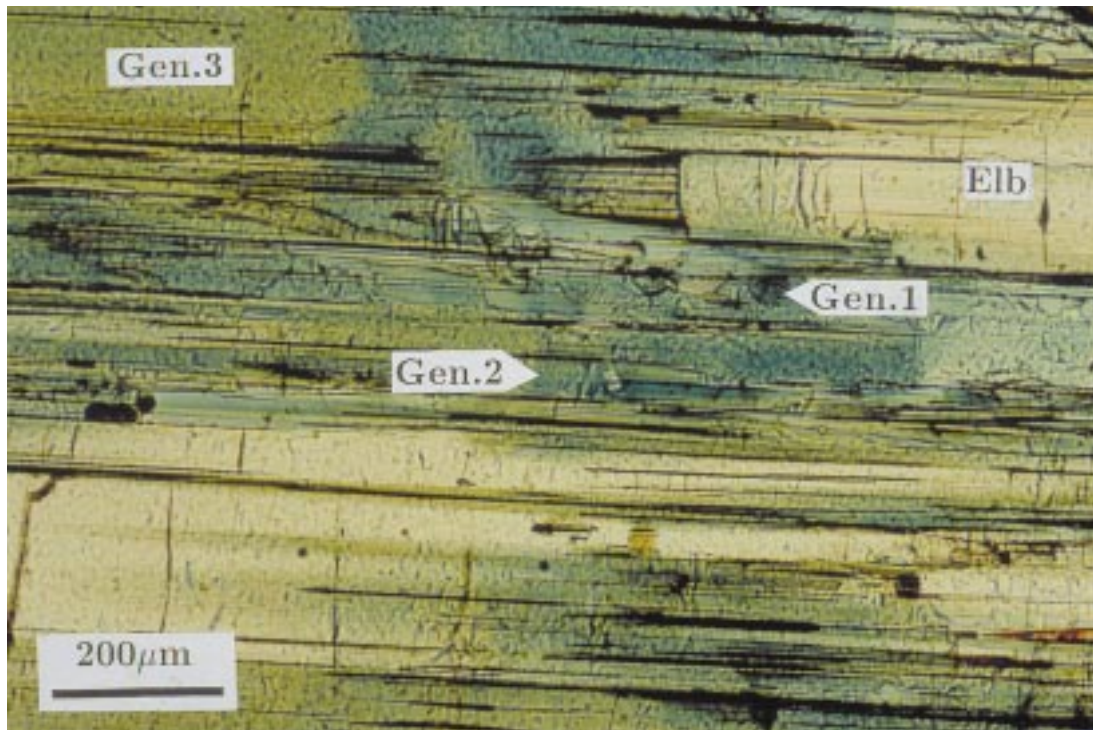


FIG. 2. Photomicrograph of fibrous tourmaline displaying the texture of the host elbaite (Elb) and three distinct generations of tourmaline growth in the fibers as observed in sections cut parallel to the fiber length. Gen. 1: Generation 1. Gen. 2: Generation 2, Gen. 3: Generation 3.

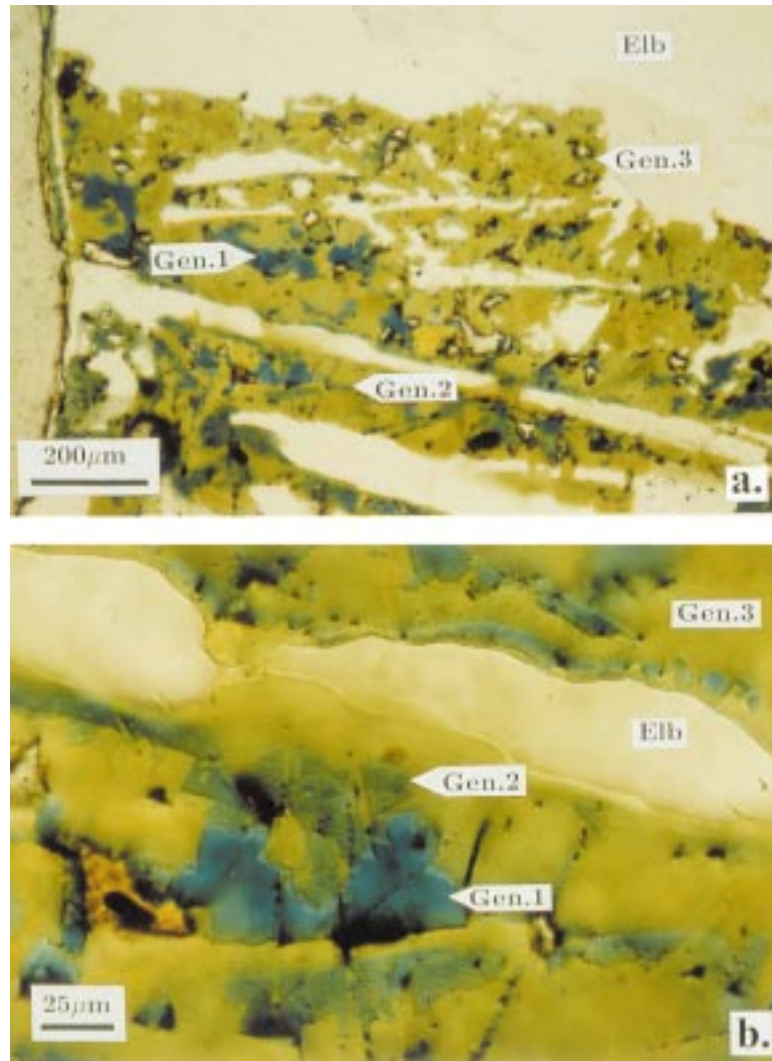


FIG. 3. Photomicrographs in plane light of sections cut perpendicular to the *c* axis of the fibers, which display host elbaite, and three generations of fiber growth. Note distinct replacement and cross-cutting relations of the three generations of fibers. (a) Tourmaline fibers exhibit a poikiloblastic relation with the elbaite host. (b) Details of earlier generations of fiber replaced by later generations. Elbaite host is colorless, Gen. 1 is dark peacock blue, Gen. 2 is lighter blue-gray, and Gen. 3 is yellowish olive green.

were used as standards. Energy-dispersion scans were done initially to define the important elements present in the tourmaline (with $Z \geq 5$). Tourmaline was quantitatively analyzed for K, Na, Ca, Fe, Mn, Mg, Ti, Al, Si, F, and Cl. The data were corrected on-line using a modified Bence-Albee correction procedure. On the basis of replicate analyses of several secondary standards, the analytical precision associated with counting statistics

(1σ) for selected oxides is estimated to be 0.21% SiO_2 , 0.13% Al_2O_3 , 0.03% TiO_2 , 0.06% FeO , 0.03% MnO , 0.11% MgO , 0.02% CaO , 0.03% Na_2O , 0.03% K_2O , 0.02% F and 0.01% Cl.

In order to calculate the stoichiometry of the tourmalines and make estimates of the amounts of undetectable light elements (Li, B, H), several assumptions were made. (1) The amount of B_2O_3 necessary to produce

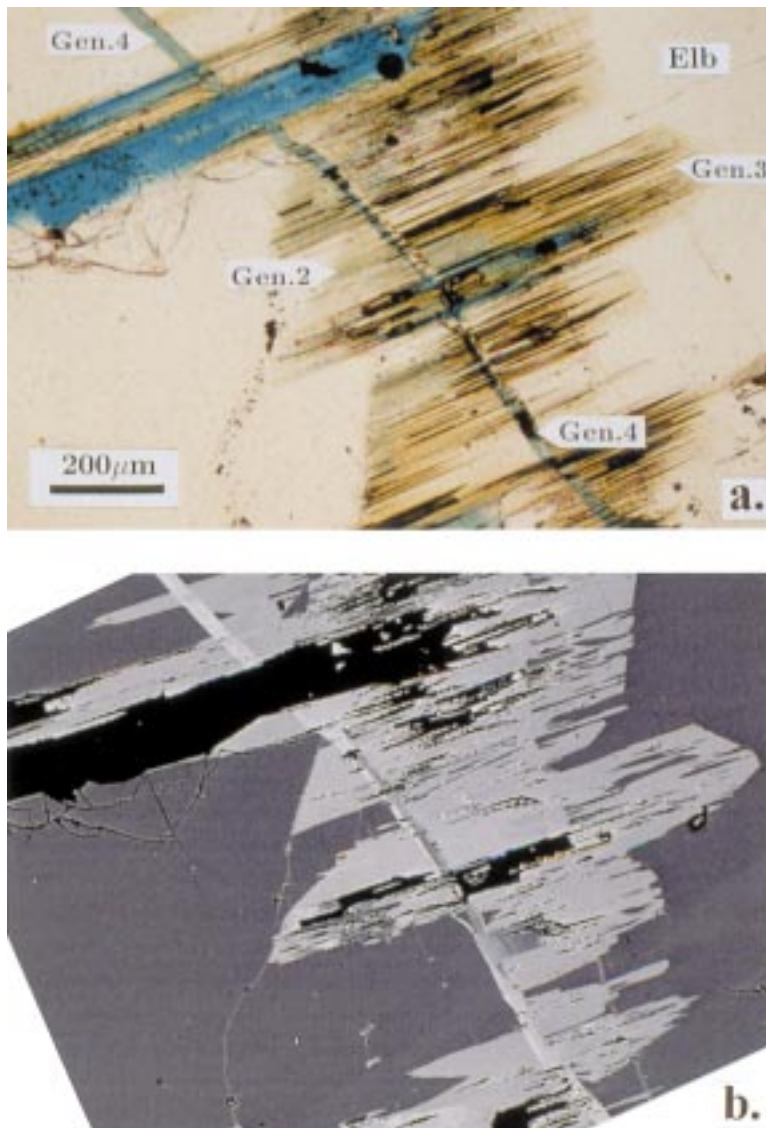


FIG. 4. Generation-4 tourmaline cuts all previous generations of fibrous growth. (a) Photomicrograph in plane light of Generation-4 tourmaline in diagonal blue vein cutting all earlier generations of tourmaline. Blue bands in upper left corner are epoxy. (b) Back-scattered electron image of the same area as shown in (a). The lighter gray tourmaline (Gen. 4), richer in Fe, clearly cuts the earlier generation. Note also the poikiloblastic nature of Gen. 3 tourmaline.

three B cations in the structural formula was calculated from stoichiometry constraints (*e.g.*, Hawthorne 1996, Bloodaxe *et al.* 1999). (2) The structural formula is based on a normalization scheme such that the proportion of Si equals 6 atoms per formula unit (*apfu*). This assumption, although likely not valid for tourmalines in

general, is a reasonable assumption in this case. On the basis of a large number of high-quality wet-chemical analyses, Povondra *et al.* (1985) demonstrated that data for elbaite from a variety of granitic pegmatites cluster very close to 6 Si *apfu*. Furthermore, a number of complete analyses (including B, Li, H analyses) of the

elbaitic tourmalines from the Cruzeiro pegmatites confirm that $\text{Si} \approx 6.0 \text{ apfu}$ is a reasonable assumption (Federico *et al.* 1998). (3) Li was estimated by subtracting the sum of the *Y*-site cations from 3, *i.e.*, assuming no vacancies in the octahedral sites (Henry & Dutrow 1996). This assumption is supported by complete chemical data obtained for other tourmalines from Cruzeiro, in which the *Y* sites are typically completely filled (Federico *et al.* 1998). (4) Fe_{tot} is assumed to be essentially all Fe^{2+} . The minor optical pleochroism present in all generations of tourmaline suggests that the Fe is mostly in a single oxidation state (*e.g.*, Henry *et al.* 1999). Determinations of Fe oxidation states in tourmalines from other pegmatite occurrences suggest the general dominance of ferrous over ferric iron (*e.g.*, Povondra *et al.* 1985, Dyar *et al.* 1998, Federico *et al.* 1998). (5) An estimate of the maximum H content is made by cat-

ion charge-balance calculations (see Henry & Dutrow 1996). If some of the iron is actually in the ferric state, the H estimate is reduced. This estimate of H, and consequently the estimate of *W*-site O^{2-} , is subject to a large uncertainty because it reflects a combination of errors associated with assumptions regarding normalization and the sum of analytical uncertainties of all measured elements. Nonetheless, this exercise is useful because one can place general limits on the *W*-site occupancy, rather than simply assume a composition in terms of the F–OH binary (*cf.* Henry & Dutrow 1996). (6) F is assumed to be exclusively accommodated in the *W* site, and any O^{2-} in the *V* and *W* sites is preferentially partitioned in the *W* site (Hawthorne & Henry 1999).

RESULTS

Growth and chemical complexity of the tourmaline fibers was initially indicated by optical properties observed in thin sections cut parallel and perpendicular to the fibers. In thin sections parallel to the fiber axis, the fibers are patchy blue to yellowish green in plane light, in contrast to the colorless host (Figs. 2, 4). The five generations of tourmaline are in optical continuity, with fiber growth parallel to the *c* axis of the host. Nucleation sites of the fibers are exclusively along the margins of the host, or within fractures.

Thin sections cut perpendicular to the fibers more clearly reveal their developmental history, as defined by distinct color-zones and cross-cutting relations (Fig. 3). Four distinct textural and compositional types comprise the fibrous tourmaline. In plane light, generation-1 tourmaline is peacock blue at maximum absorption, generation 2 is lighter blue, generation 3 is yellowish green, and generation 4 is blue. Relative growth relationships among the different generations are also distinct in BSE images (Fig. 4). Each succeeding generation partially cannibalizes and replaces the preceding generation(s) (Figs. 2, 3). A fourth generation of tourmaline cuts all previous generations remaining in optical continuity and is related to late fracture-filling event (Fig. 4).

The four generations of fiber growth, with their distinct colors and textures, generally have markedly different compositions. Chemical analyses indicate that all generations belong to either the alkali or vacancy-dominant series (Table 2, Fig. 5a). Classification on the basis of the *W*-site anion occupancy is more problematic because of uncertainty in the inferred amounts of H, but, on average, the host is part of the oxy-subgroup, generations 1, 2 and 4 are in the hydroxy-subgroup, and generation 3 is in the fluor-subgroup (Fig. 5b). The magnitude and types of additional compositional changes documented subsequently reveal information about the changing chemical environment during growth of the tourmaline. Compositional trends within and between these generations were deduced on the basis of numerous plots of chemical data; only a selected subset is shown here.

TABLE 2. AVERAGE COMPOSITION OF EACH GENERATION OF TOURMALINE, CRUZEIRO MINE, MINAS GERAIS, BRAZIL.

	Host 12*	Gen. 1 10	Gen. 2 17	Gen. 3 36	Gen. 4 1
B_2O_3 (wt%)	10.89	10.46	10.51	10.52	10.42
SiO_2	37.67 (0.28)‡	36.00 (0.19)	36.60 (0.40)	36.81 (0.43)	36.22
Al_2O_3	42.59 (0.45)	36.25 (0.88)	36.56 (0.45)	36.69 (0.76)	36.42
TiO_2	0.01 (0.01)	0.04 (0.02)	0.11 (0.03)	0.25 (0.08)	0.08
FeO	0.09 (0.06)	10.68 (0.97)	7.81 (0.63)	5.69 (0.53)	8.25
MnO	0.90 (0.14)	0.70 (0.27)	0.94 (0.09)	0.89 (0.31)	0.71
MgO	0.00	0.48 (0.11)	0.48 (0.04)	0.39 (0.13)	0.46
Li_2O^\S	1.36	0.26	0.92	1.41	0.45
CaO	0.32 (0.12)	0.04 (0.02)	0.24 (0.11)	1.16 (0.39)	0.14
Na_2O	1.76 (0.07)	1.01 (0.025)	1.90 (0.16)	2.18 (0.21)	1.68
K_2O	0.02 (0.01)	0.01 (0.01)	0.02 (0.01)	0.02 (0.01)	0.02
F	0.73 (0.11)	0.02 (0.03)	0.47 (0.19)	1.19 (0.08)	0.45
Cl	0.00	0.00	0.00	0.00	0.00
Total	96.06	95.91	96.45	96.79	95.52
O = F	0.31	0.01	0.20	0.50	0.19
TOTAL	95.75	95.90	96.25	96.29	95.33
Atomic proportions based on 6 Si cations					
B^\S (apfu)	3.000	3.000	3.000	3.000	3.000
Si	6.000	6.000	6.000	6.000	6.000
$^{\zeta}\text{Al}$	6.000	6.000	6.000	6.000	6.000
$^{\eta}\text{Al}$	1.995 (0.126)‡	1.121 (0.177)	1.064 (0.111)	1.051 (0.177)	1.110
Ti	0.001 (0.001)	0.005 (0.002)	0.014 (0.004)	0.031 (0.010)	0.010
Fe^{2+}	0.012 (0.008)	1.489 (0.138)	1.070 (0.085)	0.775 (0.070)	0.143
Mn^{2+}	0.121 (0.019)	0.099 (0.038)	0.131 (0.013)	0.123 (0.043)	0.100
Mg	0.001 (0.001)	0.119 (0.027)	0.117 (0.010)	0.094 (0.032)	0.114
Li^\S	0.870 (0.123)	0.174 (0.125)	0.604 (0.131)	0.927 (0.169)	0.523
Ca	0.055 (0.021)	0.007 (0.004)	0.043 (0.019)	0.195 (0.068)	0.025
Na	0.544 (0.021)	0.328 (0.080)	0.604 (0.051)	0.688 (0.062)	0.540
K	0.003 (0.002)	0.003 (0.002)	0.003 (0.002)	0.004 (0.002)	0.004
\square^\S	0.398 (0.019)	0.663 (0.084)	0.345 (0.068)	0.113 (0.021)	0.431
F	0.367 (0.056)	0.009 (0.013)	0.243 (0.100)	0.615 (0.042)	0.236
Cl	0.000	0.000	0.001 (0.001)	0.000	0.000
OH^\S	2.852 (0.259)	3.651 (0.304)	3.544 (0.191)	3.020 (0.315)	3.563
O^\S	0.781 (0.259)	0.340 (0.304)	0.212 (0.191)	0.365 (0.315)	0.201

* Number of analyses of each generation of tourmaline.

‡ Calculated using stoichiometric constraints (see Analytical Techniques).

§ Numbers in parentheses are standard deviations of the mean (1σ). The standard deviation with $^{\zeta}\text{Al}$ is for total Al.

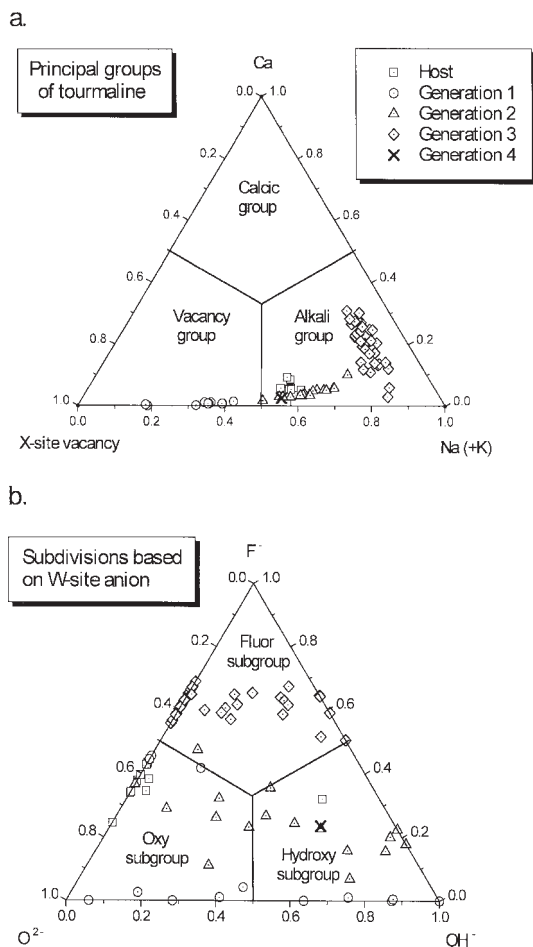


FIG. 5. General chemical groups and subdivisions of the tourmaline generations. (a) Classification of the principal groups of tourmaline based on X-site occupancy (from Hawthorne & Henry 1999). Note that generation 1 is an X-site-vacant tourmaline, whereas other generations are alkali-group tourmalines. Each symbol represents an individual composition. (b) Tourmaline-group subdivision based on anions occupying the W site. The host is restricted to the "oxy" subgroup, generation-3 tourmaline is confined to the fluor-subgroup, and generations 1 and 2 span the "hydroxy" and "oxy" subgroups. Amounts of OH and O calculated in the W site are susceptible to significant uncertainty (see section on analytical techniques).

Host

The average composition of the host is $(\text{Na}_{0.54}\text{Ca}_{0.06}\text{X}_{0.40})(\text{Li}_{0.87}\text{Fe}_{0.01}\text{Mn}_{0.12}\text{Al}_{2.00})\text{Al}_6\text{Si}_6\text{O}_{18}(\text{BO}_3)_3[(\text{OH})_{2.85}\text{O}_{0.15}](\text{F}_{0.37}\text{O}_{0.63})$, which falls in the general

category of an "oxy-elbaite" (Table 1, 2, Figs. 5, 6). However, owing to the significant proportions of X-site vacancies and F, and the roughly 1:2 ratio of Li to Al, there is almost 50% of the rossmanite component in solid solution with the "oxy-elbaite". Occurrence of this roughly binary mixture of end-member components is consistent with the supposition that owing to local bond-valence constraints, an "oxy-elbaite" tourmaline end-member is unlikely to be stable, but nevertheless can exist as a mixture with other tourmaline components up to a level of about 50% (Hawthorne 1996). The presence of significant Mn (0.12 *apfu*) and the paucity of Fe and Ti are largely responsible for the deep pink color of the elbaite (*cf.* Fritsch & Rossman 1987).

The elbaite host displays relatively minor compositional variability (Table 2, Figs. 7, 8). The most important elemental ranges involve Al (7.69–8.19 *apfu*) and F (0.25–0.44 *apfu*) (Fig. 8). Because Al is the dominant measured Y-site cation, calculated Li values are positively correlated with Al. This correlation is most consistent with the exchange vector $[\text{Li}(\text{OH})_2](\text{AlO}_2)_{-1}$ (*cf.* Burt 1989).

Generation 1

The generation-1 tourmaline fiber, characterized by irregular peacock blue patches in the fiber interior (Figs. 2–4), has a dramatically different composition than the host (Figs. 5–8). Average composition of this generation of fiber is $(\text{Na}_{0.33}\text{Ca}_{0.01}\text{X}_{0.66})(\text{Li}_{0.17}\text{Fe}_{1.49}\text{Mn}_{0.10}\text{Ti}_{0.01}\text{Al}_{1.12})\text{Al}_6\text{Si}_6\text{O}_{18}(\text{BO}_3)_3(\text{OH})_3(\text{F}_{0.01}\text{O}_{0.34}\text{OH}_{0.65})$, which is classified as foitite (Table 2, Figs. 5, 6). Relative to the host, the generation-1 tourmaline is enriched in Fe (1.48 *apfu*), OH (0.80 *apfu*) and X-site vacancy (0.27 *apfu*) and depleted in Al (0.87 *apfu*), Li (0.70 *apfu*), O (0.44 *apfu*), F (0.36 *apfu*), and Na (0.22 *apfu*). The compositional transition from the host to the first-generation fiber can be primarily described in terms of the exchange vectors $\text{Fe}_2(\text{LiAl})_{-1}$ and $\text{OH}(\text{F})_{-1}$ (Figs. 7a, b).

This first generation of fibrous growth exhibits moderate compositional variability. Among the elements sought, the greatest ranges are observed for Al (6.81–7.35 *apfu*), Fe (1.35–1.76 *apfu*) and Na (0.18–0.42 *apfu*; Figs. 5–8). Comparable variability is developed in calculated Li values (0.00–0.34 *apfu*) and X-site vacancies (0.57–0.81). Consequently, compositional heterogeneity of the first generation of fiber is best described by the exchange vectors $\text{NaLi}(\square\text{Fe})_{-1}$ and $[\text{Li}(\text{OH})_2](\text{AlO}_2)_{-1}$ (Figs. 7a, b, 8a). A notable feature in this generation of alkali-deficient tourmaline is the paucity of F in an environment that was otherwise F-rich (Fig. 8b). The composition of this early-formed tourmaline fiber is similar to that of fibrous foitite described from other pegmatite localities (*e.g.*, Pezzotta *et al.* 1996, Aurisicchio *et al.* 1997).

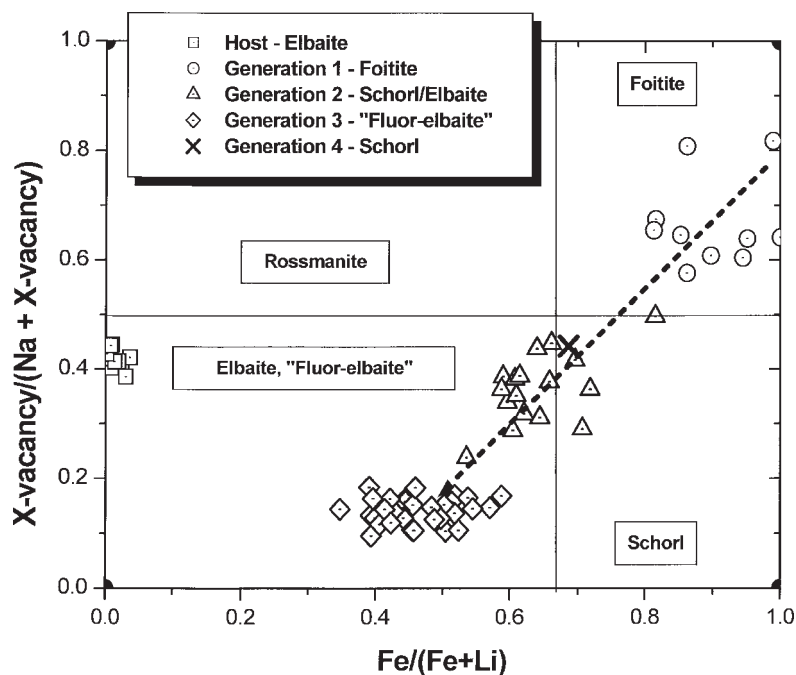


FIG. 6. Classification of the host tourmaline and Generations 1 to 4 fibers. Lines dividing the diagram represent 50% of the end-member components. The host falls within the elbaite field but, on the basis of the dominance of O in the W site, it is best classified as an "oxy-elbaite". Generation-1 tourmaline falls entirely in the foitite field. Generations 2 and 4 fall on the boundary between elbaite and schorl and are, on average, hydroxy-tourmalines, and can be classified as Fe-rich elbaite to Li-rich schorl. Generation-3 tourmaline, in the F-subgroup, falls within the elbaite field and is best termed a "fluor-elbaite". The dashed arrow represents the general compositional trend followed by fibers of generations 1 to 3.

Generation 2

The second generation of fibrous tourmaline, developed as blue-gray patches that locally cross-cut and replace generation-1 tourmaline, is compositionally distinct from the latter. With an average composition of $(\text{Na}_{0.60}\text{Ca}_{0.04}\text{X}_{0.36}) (\text{Li}_{0.60}\text{Fe}_{1.07}\text{Mn}_{0.13}\text{Mg}_{0.12}\text{Ti}_{0.01}\text{Al}_{1.06}) \text{Al}_6\text{Si}_6\text{O}_{18} (\text{BO}_3)_3 (\text{OH})_3 (\text{F}_{0.24}\text{O}_{0.21}\text{OH}_{0.55})$, it is best classified as Fe-rich elbaite to Li-rich schorl (Fig. 6, Table 2). Relative to generation-1 tourmaline, the average composition is enriched in Li (0.43 *apfu*), Na (0.28 *apfu*), and F (0.23 *apfu*) and depleted in Fe (0.42 *apfu*), X-site vacancies (0.32 *apfu*), O (0.13 *apfu*) and OH (0.11 *apfu*). Changes from generation 1 to generation 2 are most consistent with operation of the exchange vectors $\text{NaLi}(\square\text{Fe})_{-1}$ and $\text{F}(\text{OH})_{-1}$ (Figs. 7a, b) similar to general evolutionary trends developed in many pegmatite systems (e.g., London 1999).

The amount of compositional variability of generation-2 tourmaline is similar to that observed within generation-1 tourmaline. Among the elements sought, the

greatest ranges include Al (6.85–7.25 *apfu*), F (0.11–0.47 *apfu*), Fe (0.86–1.25 *apfu*) and Na (0.50–0.66 *apfu*) (Figs. 5–8). Comparable variability is developed in the calculated Li values (0.29–0.78 *apfu*) and X-site vacancies (0.21–0.48). Variability within generation-2 tourmaline is best described by the exchange vectors $\text{NaLi}(\square\text{Fe})_{-1}$, $(\text{Li}(\text{OH})_2)(\text{AlO}_2)_{-1}$ and $\text{F}(\text{OH})_{-1}$ (Figs. 7a, b, 8a, b).

Generation 3

The third generation is a yellowish to olive green poikiloblastic tourmaline that replaces earlier generations of fibers as well as the host, and is compositionally distinct from all other generations. Generation-3 tourmaline has an average composition of $(\text{Na}_{0.69}\text{Ca}_{0.20}\text{X}_{0.11}) (\text{Li}_{0.93}\text{Fe}_{0.78}\text{Mn}_{0.12}\text{Mg}_{0.09}\text{Ti}_{0.03}\text{Al}_{1.05}) \text{Al}_6\text{Si}_6\text{O}_{18} (\text{BO}_3)_3 (\text{OH})_3 (\text{F}_{0.62}\text{O}_{0.36}\text{OH}_{0.02})$, and is best classified as Fe-rich "fluor-elbaite" (Figs. 5, 6, Table 2). It is the most F-rich of the four generations of fiber, reaching nearly a full complement of F atoms in the W site

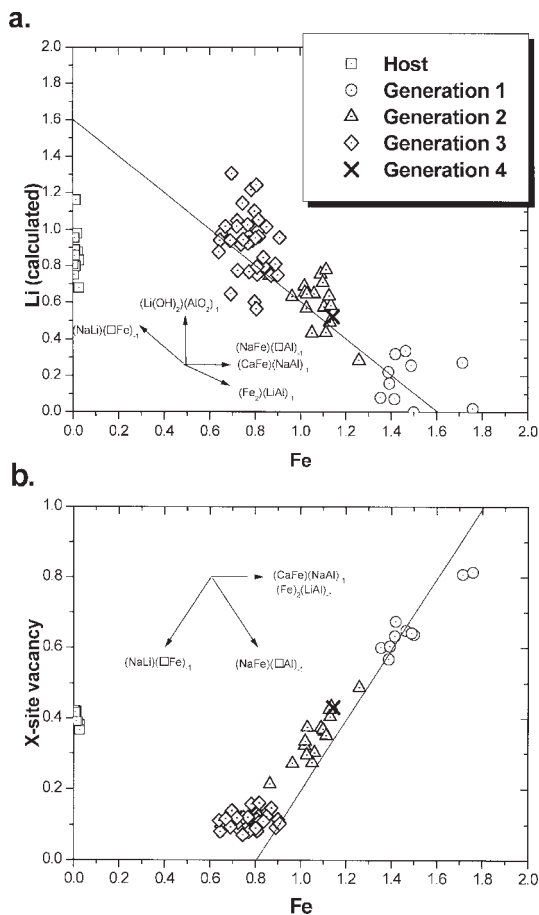


FIG. 7. Relationship between Fe and Li or X-site vacancy for all generations of tourmaline. Arrows labeled with the exchange vectors represent directions of the vector but not the magnitude. (a) Fe versus calculated Li. Reference line has a slope of -1 , consistent with the exchange vector $(\text{NaLi})(\square\text{Fe})_{-1}$. The compositional progression of generation-1 to generation-3 tourmaline generally follows this exchange vector. (b) Fe versus X-site vacancy. Reference line has a slope of $+1$, consistent with the exchange vector $(\text{NaLi})(\square\text{Fe})_{-1}$ with the progression of generations 1 to 3.

(Fig. 8b). It is also the most Fe-poor of the four generations (Figs. 7a, b, 8a, b), and contains a nearly filled X site, having substantial variability with respect to Ca and Na (Figs. 5, 7b). The constant but low X-site vacancy is commensurate with an increase in F (Figs. 5, 7b, 8b). Relative to generation-2 tourmaline, the average generation-3 composition displays an increase in F (0.37 *apfu*), Li (0.32 *apfu*), Ca (0.15 *apfu*), Na (0.08 *apfu*), and O (0.15 *apfu*) and a decrease in OH (0.52 *apfu*), Fe (0.30 *apfu*), and X-site vacancy (0.23) (Figs. 5–8).

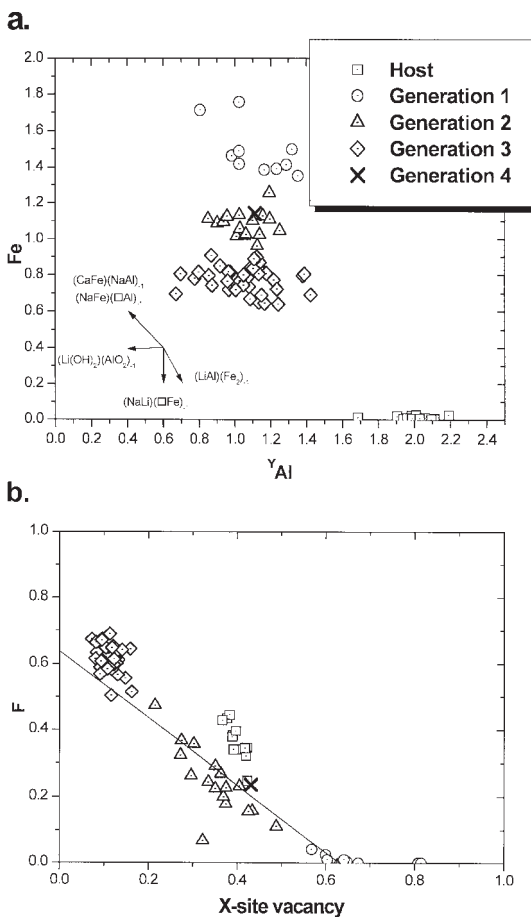


FIG. 8. Al-Fe and X-site vacancy - F relations in all generations of tourmaline. Arrows labeled with the exchange vectors represent the direction (not the magnitude) of the vector. (a) ⁷Al versus Fe. Separation of Generations 1–3 is generally consistent with the exchange vector $(\text{NaLi})(\square\text{Fe})_{-1}$, but there is also dispersion of the data within each generation roughly parallel with $[\text{Li}(\text{OH})_2](\text{AlO}_2)_{-1}$. (b) X-site occupancy versus F. Reference line has a slope of -1 . All generations of tourmaline, including the pink tourmaline host, generally follow this line, suggesting an X-site vacancy - F avoidance. The line also implies that F should be essentially absent in tourmalines with more than 0.5 *apfu* X-site vacancy.

These general changes from generation 2 to generation 3 are most consistent with the exchange vectors $\text{NaLi}(\square\text{Fe})_{-1}$ and $\text{F}(\text{OH})_{-1}$.

Generation-3 tourmaline is the most heterogeneous of the four generations, with the greatest ranges involving Al (6.67–7.42 *apfu*), Fe (0.64–0.91 *apfu*), Ca (0.03–0.31 *apfu*), Na (0.58–0.82 *apfu*), and F (0.50–0.69 *apfu*) (Figs. 5–8). Comparable variability is developed in cal-

culated values for Li (0.56–1.24 *apfu*), OH (0–0.50 *apfu*), and O (0–0.44 *apfu*). As such, chemical variability within this generation is primarily due to the $[\text{Li}(\text{OH})_2](\text{AlO}_2)_{-1}$ substitution, with minor $\text{CaFe}(\text{NaAl})_{-1}$ (Figs. 7a, 8a).

Generation 4

The fourth generation of tourmaline appears as a late fracture-filling unrelated to the earlier generations. This fracture filling cuts all previous generations of fibers as well as the host. Compositionally, generation-4 tourmaline is a lithian schorl with an average composition indistinguishable from that of generation-2 tourmaline (Table 2, Fig. 6). Relative to generation-3 tourmaline, the generation-4 tourmaline exhibits an increase in Fe, X_{\square} and a decrease in F.

DISCUSSION

The complexity of the fiber zoning, the alternating periods of chemically distinct growth interrupted by periods of dissolution and the radical change in compositions between growth stages, are suggestive of open-system behavior (*e.g.*, Orlandi & Pezzotta 1996, London 1999). This pattern, coupled with the overall compositions of Cruzeiro tourmaline, is most consistent with tourmaline growth in a pegmatite pocket.

The punctuated optical and chemical progression of different generations of tourmaline marks distinct evolutionary periods in the chemical history of the cavity that hosted the tourmaline system. Tourmaline fibers appear to record changes in fluid composition in the local environment of the growing and dissolving tourmaline. Initially, the fibrous tourmaline nucleated and partially replaced the host tourmaline. This was followed by three periods of partial dissolution prior to new growth. Local dissolution of the fibers must represent periods when the existing tourmaline was no longer in equilibrium and became destabilized by the fluid, likely by a more alkaline fluid (*e.g.*, London *et al.* 1996) or a fluid with different relative concentrations of ions (especially Na^+) (*e.g.*, Dutrow *et al.* 1999). An influx, or multiple influxes, of new out-of-equilibrium fluids would drive dissolution. Alternatively, other mineral reactions in the pegmatite pocket, such as growth of albite, could change the local composition of the fluid, thus destabilizing pre-existing tourmaline. When fluids were saturated with components necessary for tourmaline precipitation, growth once again commenced. The growth of markedly different compositions suggests that a compositionally distinct fluid was associated with each stage of tourmaline growth. At least some of the boron required for new growth was likely provided by dissolution of the destabilized tourmaline.

The “oxy-elbaite” – rossmanite host is a relatively homogeneous Li-, F-, and Al-rich tourmaline, which reflects extensive fractionation typical of granitic peg-

matite fluids in the late stages of crystallization (*cf.* London *et al.* 1996). In general, this tourmaline must have been in equilibrium with an aqueous magmatic fluid that not only was enriched in Li and F, but also was deficient in Na and Fe. Federico *et al.* (1998) noted that the ubiquitous assemblage of muscovite and tourmaline indicates the peraluminous character of the early pegmatite-forming melts at the Cruzeiro mine. They considered the compositional variations of the tourmaline from the margin to the core to reflect a disequilibrium fractional crystallization process through liquid undercooling at decreasing temperature.

Development of the initial fibers of tourmaline (generation 1), now preserved only in the fiber interiors, followed a dramatic change in tourmaline composition that must reflect a complementary modification in the fluid phase, relative to the original magmatic fluids. Most likely these tourmaline-forming fluids were restricted to a pegmatite pocket where fluid influx could dramatically alter the equilibrium tourmaline composition. This generation of tourmaline shifts compositionally such that Fe and OH substantially increase at the expense of Al, Na, Li, F, and O, roughly in accordance with the exchange vectors $\text{Fe}_2(\text{LiAl})_{-1}$ and $\text{OH}(\text{F})_{-1}$. Remarkably small amounts of F in the foitite do not necessarily reflect low F in the fluid. Instead, they more likely are a function of crystal-chemical constraints involving significant X-site vacancies that preclude abundant F in the tourmaline structure (Robert *et al.* 1998, Henry & Hawthorne 1999). Compositionally distinct fluids derived from the evolving magma (*cf.* Aurisicchio *et al.* 1997) may have infiltrated during rupture of an isolated pegmatite pocket to cause the generation-1 fibers. There must have been an influx of reactive fluid richer in Fe and poorer in Na into the local region to alter the tourmaline composition. A decrease of Na in the fluid could be attained with the crystallization of albite in the pocket. An increase in Fe could be due to the breakdown of other Fe-bearing phases, although garnet and tourmaline are the only major Fe-bearing phases recorded in the pegmatite. This is the mechanism that Aurisicchio *et al.* (1997) proposed to explain the formation of late-generation fibrous foitite in Elba pegmatites. They noted that the biotite breaks down to form muscovite and clay minerals. However, in the case of the tourmaline fibers in this study, the fiber compositions continued to change following the formation of foitite, incorporating the complexity of a late fractionating fluid phase.

Successively later generations (1–3) of tourmaline display a discontinuous but progressive enrichment in Na, Li, F, and late Ca, implying that reacting fluids were successively enriched in these components during crystallization. Na enrichment could be due to the breakdown of albite coincident with other Na, Li-bearing phases (*e.g.*, amblygonite). This increase is suggestive of fractionation and is analogous to the overall magmatic fractionation trend of the pegmatite. This finding also

supports the idea that the fluid may have been isolated in the pocket during growth of generations 1–3, allowing fractionation to proceed. It is possible that local fractionation developed after initial pocket rupture and subsequent isolation until a later pocket rupture led to the development of generation-4 tourmaline.

Generation-4 Li-rich schorl likely records a period when the entire cavity fractured along with all of the preceding generations of tourmaline, and new fluid was introduced. This influx of fluid associated with a late-stage episode of fracturing, after primary tourmaline crystallization had ceased, may correspond to the change from orthomagmatic to host-rock-controlled hydrothermal fluid. The commonly observed warping and fracturing of minerals throughout the pegmatite are likely related to this period (Cassedanne *et al.* 1980). Thus, at least two influxes of compositionally distinct fluids are required to explain the resulting compositional spectrum of the tourmaline at Cruzeiro, and as many as four influxes are possible.

Compositional changes in successive generations of fiber growth not only record the influences of the evolving fluids in the pegmatite, but also reflect crystal-chemical constraints. Several of the constraints observed here have been previously elucidated on the basis of crystal-structure refinements and detailed chemical analyses (*e.g.*, Hawthorne 1996, Henry & Hawthorne 1999). A particularly noteworthy feature of the chemical variations involving all generations of tourmaline is the roughly inverse relationship between F and X-site vacancies, *i.e.*, F – X-site vacancy avoidance (Fig. 8b). Thus X-site vacancies place crystal-chemical constraints on the extent of incorporation of F in the tourmaline structure, and X-site-vacant tourmalines such as foitite and rossmanite are unlikely to contain significant amounts F (*cf.* Robert *et al.* 1998, Henry & Hawthorne 1999). Such crystal-chemical influences should be considered when attempting to estimate F in the fluid phase from mineral chemistry.

In this study, we demonstrate that even a single fiber of tourmaline can record distinct and complex compositional changes that monitor evolving fluids associated with growth, and that infiltration of fluids far-from-equilibrium may be intermittently associated with pegmatite genesis. In addition, this dramatic record of compositional evolution in tourmaline fibers may mark the transition from magmatic to hydrothermal conditions in granitic pegmatites.

ACKNOWLEDGEMENTS

BLD thanks with the Department of Earth and Planetary Sciences at the University of New Mexico and the Institute of Geophysics and Planetary Physics at Los Alamos National Laboratory for facilities and a fabulous working environment during a sabbatical leave. Our investigations were also supported by NSF grants EAR-9220195 and EAR-9814418 (BLD) and EAR-

9405747 (DJH). Rick Young is thanked for his remarkable job in making thin sections containing mineral fibers. An especially thorough and helpful review by John Slack greatly improved the manuscript. Additional thanks are due to R.V. Dietrich and Bob Martin, who shared their insights and improved the manuscript. However, the interpretations here are those of the authors, and not necessarily shared by the reviewers.

REFERENCES

- AURISICCHIO, C., OTTOLINI, L. & PEZZOTTA, F. (1997): Electron and ion microprobe analyses, paragenesis, and genetic inferences of foitite of Elba Island (Italy). *Tourmaline 1997, Int. Symp. on Tourmaline, Abstr. Vol.*, 117-118.
- BANTLY, A.W. (1964): Tourmaline whiskers. *Rocks and Minerals* **39**, 138-140.
- BLOODAXE, E.S., HUGHES, J.M., DYAR, M.D., GREW, E.S. & GUIDOTTI, C.V. (1999): Linking structure and chemistry in the schorl–dravite series. *Am. Mineral.* **84**, 922-928.
- BURT, D.M. (1989): Vector representation of tourmaline compositions. *Am. Mineral.* **74**, 826-839.
- CASSEDANNE, J. P., CASSEDANNE, J. O. & SAUER, D. A. (1980): The Cruzeiro mine past and present. *Mineral. Rec.* **11**, 363-370.
- COELHO, I.S. (1948): Turmalina fibrosa da “Mina do Cruzeiro,” Santa Maria do Suassui, Minas Gerais. *Mineração Metal.* **13**, 49-53.
- DIETRICH, R.V. (1985): *The Tourmaline Group*. Van Nostrand Reinhold Co., New York, N.Y.
- DUTROW, B.L., FOSTER, C.T., JR. & HENRY, D.J. (1999): Tourmaline-rich pseudomorphs in sillimanite zone metapelites: demarcation of an infiltration front. *Am. Mineral.* **84**, 794-805.
- DYAR, M.D., TAYLOR, M.E., LUTZ, T.M., FRANCIS, C.A., GUIDOTTI, C.V. & WISE, M. (1998): Inclusive chemical characterization of tourmaline: Mössbauer study of Fe valence and site occupancy. *Am. Mineral.* **83**, 848-864.
- FEDERICO, M., ANDREOZZI, G. B., LUCCHESI, S., GRAZIANI, G. & CÉSAR-MENDES, J. (1998): Compositional variation of tourmaline in the granitic pegmatite dykes of the Cruzeiro mine, Minas Gerais, Brazil. *Can. Mineral.* **36**, 415-431.
- FOIT, F.F., JR., FUCHS, Y. & MYERS, P.F. (1989): Chemistry of alkali-deficient schorls from two tourmaline–dumortierite deposits. *Am. Mineral.* **74**, 1317-1324.
- FRICTSCH, E. & ROSSMAN, G.R. (1987): An update on color in gems. I. Introduction and color caused by dispersed metal ions. *Gems and Gemology* **23**, 126-139.
- FURBISH, W.J. (1968): Tourmaline of acicular and filiform morphology from pyrophyllite deposits of North Carolina. *Rocks and Minerals* **43**, 584-586.

- HAWTHORNE, F.C. (1996): Structural mechanisms for light-element variations in tourmaline. *Can. Mineral.* **34**, 123-132.
- _____ & HENRY, D.J. (1999): Classification of the minerals of the tourmaline group. *Eur. J. Mineral.* **11**, 201-215.
- HENRY, D.J. & DUTROW, B.L. (1992): Tourmaline in a low-grade clastic metasedimentary rock: an example of the petrogenetic potential of tourmaline. *Contrib. Mineral. Petrol.* **112**, 203-218.
- _____ & _____ (1996): Metamorphic tourmaline and its petrologic applications. In *Boron: Mineralogy, Petrology, and Geochemistry* (E.S. Grew & L.M. Anovitz, eds.). *Rev. Mineral.* **33**, 503- 557.
- _____ & GUIDOTTI, C.V. (1985): Tourmaline as a petrogenetic indicator mineral: an example from the staurolite-grade metapelites of NW Maine. *Am. Mineral.* **70**, 1-15.
- _____ & HAWTHORNE, F.C. (1999): Tourmaline – what's in a name? *Geol. Soc. Am., Abstr. Programs* **31**, A357.
- _____, KIRKLAND, B.L. & KIRKLAND, D.W. (1999): Sector-zoned tourmaline from the cap rock of a salt dome. *Eur. J. Mineral.* **11**, 263-280.
- IYENGAR, K.Y.S. (1937): Fibrous tourmalines from the Mysore State. *Current Sci. (India)* **5**, 534- 535.
- LONDON, D. (1999): Stability of tourmaline in peraluminous granite systems: the boron cycle from anatexis to hydrothermal aureoles. *Eur. J. Mineral.* **11**, 253-262.
- _____, MORGAN, G.B., IV & WOLF, M.B. (1996): Boron in granitic rocks and their contact aureoles. In *Boron: Mineralogy, Petrology, and Geochemistry* (E.S. Grew & L.M. Anovitz, eds.). *Rev. Mineral.* **33**, 299-330.
- LYCKBERG, P. & HAWTHORNE, F.C. (1997): Foitite from the Kazionnitsa pegmatite, Alabashka pegmatite field, Ural Mountains, Russia. *Tourmaline 1997, Int. Symp. on Tourmaline, Abstr. Vol.*, 68-69.
- MITCHELL, R.S. (1964): Matted filiform tourmaline from Amelia County, Virginia. *Rocks and Minerals* **39**, 236-237.
- MODRESKI, P. J., FOORD, E.E. & BARBOSA, C.P. (1997): Crystal chemistry of uvite–dravite from the Brumado magnesite deposits, Bahia, Brazil. *Tourmaline 1997, Int. Symp. on Tourmaline, Abstr. Vol.*, 59-60.
- NOVÁK, M. (1998): Blue dravite as an indicator of fluid composition during subsolidus replacement processes in Lipoor granitic pegmatites in the Moldanubicum, Czech Republic. *J. Czech Geol. Soc.* **43**, 24-30.
- _____ & ŽÁK, K. (1970): Dravite asbestos from Chvaletice. *Acta Univ. Carol., Geologica* **1**, 27- 44.
- ORLANDI, P. & PEZZOTTA, F. (1996): *Minerali dell'Isola d'Elba*. Edzioni Novecento Grafico, Bergamo, Italy.
- PEZZOTTA, F., HAWTHORNE, F.C., COOPER, M.A. & TEERTSTRA, D.K. (1996): Fibrous foitite from San Piero in Campo, Elba, Italy. *Can. Mineral.* **34**, 741-744.
- POVONDRA, P., ČECH, F. & STANĚK, J. (1985): Crystal chemistry of elbaites from some lithium pegmatites of the Czech massif. *Acta Universitatis Carolinae – Geologica* 1985, 1-24.
- RAMA SWAMY, S. & IYENGAR, K.Y.S. (1937): X-ray analysis of the structure of a fibrous modification of tourmaline. *Indian Acad. Sci. Proc.* 419-422.
- ROBERT, J.-L., DELLA VENTURA, G., DELBOVE, F., DIAZ, M., GOURDANT, J.-P., PAPIN, A. & SERGENT, J. (1998): Structural control of the OH → F exchange in rock-forming hydrous silicates: a review based on experimental and spectroscopic data. *Int. Mineral. Assoc., 17th Gen. Meeting (Toronto), Abstr. Programme*, A98.
- SKINNER, H.C.W., ROSS, M. & FRONDEL, C. (1988): *Asbestos and Other Fibrous Materials. Mineralogy, Crystal Chemistry and Health Effects*. Oxford University Press, New York, N.Y.
- ŠREIN, V., LITOCHEB, J., ŠJKORA, J., ŠREINOVA, B. & PIVEC, E. (1997): Fibrous dravite from quartz lode near Krasovice in central Bohemia. *Tourmaline 1997, Int. Symp. on Tourmaline, Abstr. Vol.*, 99-100.

Received May 27, 1999, revised manuscript accepted February 1, 2000.

